Vol 18 No 11, November 2009
1674-1056/2009/18(11)/4852-13

Chinese Physics B

© 2009 Chin. Phys. Soc.
and IOP Publishing Ltd

Modelling of a DNA packaging motor*

Qian Jun(钱 钧)[a], Xie Ping (谢 平)[b]†,
Xue Xiao-Guang(薛晓光)[c], and Wang Peng-Ye(王鹏业)[b]

[a] *College of Physics Science, Nankai University, Tianjin* 300071, *China*
[b] *Laboratory of Soft Matter Physics, Institute of Physics, Chinese Academy of Sciences, Beijing* 100190, *China*
[c] *Department of Physics, Renmin University of China, Beijing* 100872, *China*

(Received 6 April 2009; revised manuscript received 7 May 2009)

During the assembly of many viruses, a powerful molecular motor packages the genome into a preassembled capsid. The Bacillus subtilis phage ϕ29 is an excellent model system to investigate the DNA packaging mechanism because of its highly efficient *in vitro* DNA packaging activity and the development of a single-molecule packaging assay. Here we make use of structural and biochemical experimental data to build a physical model of DNA packaging by the ϕ29 DNA packaging motor. Based on the model, various dynamic behaviours such as the packaging rate, pause frequency and slip frequency under different ATP concentrations, ADP concentrations, external loads as well as capsid fillings are studied by using Monte Carlo simulation. Good agreement is obtained between the simulated and available experimental results. Moreover, we make testable predictions that should guide future experiments related to motor function.

Keywords: DNA translocation, pause, slip, molecular motor
PACC: 3620, 8715B, 8715H, 8715K

1. Introduction

Many viruses, including herpesvirus, poxvirus, adenovirus, and double-stranded deoxyribonucleic acid (DNA) bacteriophages package the genome into empty capsids using packaging motors powered by the hydrolysis of adenosine triphosphate (ATP).[1,2] The Bacillus subtilis bacteriophage ϕ29 is an excellent system to investigate the DNA packaging mechanism.[3−5] The molecular motor of ϕ29 is composed of three components: (i) a dodecameric head-tail connector,[6,7] gene product 10 (gp 10); (ii) a ring comprised of five[6,8] or six[9−13] copies of the 174-base prohead ribonucleic acid (RNA) (pRNA) bound to the connector; and (iii) multiple copies of the ATPase gp16 that interacts with the pRNA.[6,14] It is believed that gp16 has the same copy number as the pRNA, likely acting as a complex of heterodimers (pRNA-ATPase).[3]

The ϕ29 DNA packaging motor is among the strongest motors known, with a stalling force of more than 50 pN and an initial velocity of about 100 bp/s (1 bp=0.34 nm) under low external loads. Recent single-molecule studies of ϕ29 motor have elucidated many details of the packaging process.[4,5] The packaging rate of the motor depends on the concentrations of ATP and adenosine diphosphate (ADP), and it decreases with increasing load or with increasing capsid filling. Pauses and slips also occur in the packaging process. The pause frequency increases with higher capsid fillings while the pause duration (mean time 4 s) is not strongly correlated with the filling. The slip frequency increases with rising applied external force, and decreases with increasing concentration of ATP. Movements of over 5 μm have been observed, indicating high processivity of the motor.

Many theoretical models[5−7,15−26] of viral DNA packaging have been proposed. Early models supposed that the DNA translocation is coupled with the rotation of the head-tail connector dodecamer[6,7] — an idea first introduced by Hendrix.[15] However, recent experimental results[27] excluded connector rotation with a very high probability. Recently, a simple model was proposed by Chemla *et al*,[5] in which the translocation of DNA is performed by the ring of ATPases via a conformational change induced by ATP hydrolysis. With the model, most of the experimental data have been well simulated. Nevertheless, the detailed origin of pause and slip is still not very clear and a unified mechanism for packaging, pause and slip is desired.

In this work, we make use of structural and bio-

*Project supported by the National Natural Science Foundation of China (Grant Nos 10834014 and 10674173) and the National Basic Research Program of China (Grant No 2009CB930704).
†Corresponding author. E-mail: pxie@aphy.iphy.ac.cn

chemical experimental data to build a new physical model of DNA translocation by the ϕ29 DNA packaging motor. Based on the model, various experimental results on DNA packaging velocity, pause frequency and slip frequency are reproduced very well by using Monte Carlo simulation. We also present the model's prediction of the slip and pause frequency at different values of [ATP], [ADP] and external force.

2. Model

2.1. Basic assumptions

Whether the pRNA ring of the ϕ29 DNA packaging motor is a hexamer or a pentamer is under debate.[8,9,12] However, many experiments report that only the hexameric pRNA ring is active in DNA packaging[10,12,13] and, before and during DNA translocation, the pRNA ring is a hexamer assembled from dimers.[12] Thus, in this work, it is supposed that the active form of the motor has a hexameric structure of pRNA rather than a pentameric structure.

Our proposed model is constructed based on the following three assumptions.

Assumption 1 Nucleotide-state-dependent binding affinity for DNA. Experimental results showed that the affinity of the ϕ29 packaging motor for DNA is high in the ATP state while it is low in the ADP or nucleotide-free state.[5] Other ring-shaped hexameric motor proteins also show similar nucleotide-dependent binding affinity. For example, it has been shown that RuvB binds strongly DNA in the presence of ATP or a nonhydrolyzable ATP analogue ATPγS, while no interaction between RuvB and DNA in the presence of ADP or in the absence of nucleotide was detected.[28] Moreover, experimental results on hexameric T7 gp4 helicase indicated that it has a high affinity for DNA in the presence of 2'-deoxythmidine 5'-triphosphate (dTTP), a low affinity in the presence of 2'-deoxythymidine 5-diphosphate (dTDP) and a very low affinity in the absence of nucleotides.[29] Based on this evidence, we make the following hypothesis for a pRNA-ATPase subunit of the ϕ29 packaging motor: (A) a weak DNA-binding ATP state (unactivated Subunit.ATP complex), (B) a strong DNA-binding ATP state (activated Subunit*.ATP complex), (C) a strong DNA-binding adenosine diphosphate and inorganic phosphate (ADP.Pi) state (Subunit.ADP.Pi complex), (D) a weak DNA-binding ADP state, and (5) a very weak DNA-binding nucleotide-free state, with negligibly small binding affinity. Note here that, as proposed by Chemla *et al*,[5] we also supposed that there exists a weak DNA-binding ATP state (unactivated Subunit.ATP complex) besides the strong DNA-binding ATP state (activated Subunit*.ATP complex). Moreover, to be consistent with the experimental results for T7 helicase,[29] it is proposed that the subunit.ADP complex has a larger binding affinity for DNA than a nucleotide-free subunit.

Assumption 2 Sequential ATPase activities around the ring. Similar to other ring-shaped motor proteins such as hexameric T7 helicase[30−32] and the bacteriophage ϕ12 P4 RNA packaging hexamer[33,34] that show sequential ATPase activities around the ring in the presence of DNA or RNA, it is reasonable to assume that the ATPase activity around the pRNA ring is also sequential in the presence of DNA, which is detailed as follows. The strong binding of DNA to a Subunit*.ATP complex (e.g., subunits 1 in Fig.1(a)) stimulates (i) the ATP hydrolysis in and inorganic phosphate (Pi) release from the catalytic site of the subunit (e.g., subunits 1) and (ii) the transitions of Subunit.ATP to activated Subunit*.ATP in the next adjacent subunit (e.g. subunit 2 in Fig.1(c)) in a counterclockwise direction. This assumption is consistent with the biochemical experiment showing that the basal ATPase activity of p16 is very low, but is stimulated 10–20-fold by nucleic acids.[35] A similar hypothesis has also been used for modelling hexameric T7 helicase[36] and RuvB protein.[37] The coordination of ATPase activities requires structural elements for communication between adjacent ATPase subunits. Recent studies of the crystal structure of motor proteins such as T7 helicase,[38] P4 portal protein[33] and RuvB[39] found that the 'arginine fingers' (Arg279 in P4, Arg522 in T7 helicase and Arg174 in RuvB) between adjacent subunits of the hexamer contribute to transducing conformational changes. Thus, we infer that similar finger residues in ϕ29 hexamer contribute to the coordination of ATPase activities between adjacent subunits. This assumption is also consistent with the proposal by Chemla *et al*[5] that DNA translocation must involve at least two subunits and the activities of these two ATPase must be coordinated.

Assumption 3 Hydrolysis of ATP to ADP.Pi inducing the power stroke. Recently determined snapshots of the crystal structure of the ϕ12 P4 RNA packaging hexamer in different nucleotide

states[33] revealed that the putative RNA binding residue is displaced along the channel following the hydrolysis of bound ATP. The crystal structure of the active T7 helicase hexamer with different nucleotides in different subunits also revealed that nucleoside triphosphate (NTP) hydrolysis triggers a 15° rotation of that subunit in the plane of the ring, putatively displacing the DNA-binding loop by 6–7 Å (1 Å=0.1 nm) along the axis of the hexamer.[30] Since no similar snapshots of the crystal structure are available for the ϕ29 DNA packaging hexamer, we assume that the ATP hydrolysis in a ϕ29 subunit also causes DNA-binding residue movement by a distance L, to be consistent with the observations for the ϕ12 P4 RNA packaging hexamer and the T7 helicase hexamer. It is noted here that the strong bindings of pRNA-ATPase subunit with DNA in both the activated Subunit*.ATP and Subunit.ADP.Pi complexes (see Assumption 1) ensure an effective displacement of DNA. An important point that should be pointed out is that this proposal of ATP hydrolysis inducing power stroke is different from that of Pi release inducing power stroke in Ref.[5]. As just mentioned, the present proposal is inferred from crystal studies of the ϕ12 P4 RNA packaging motor and of the T7 helicase hexamer. However, it will be noted that, in our model, the two different proposals should give the same results for the packaging dynamics.

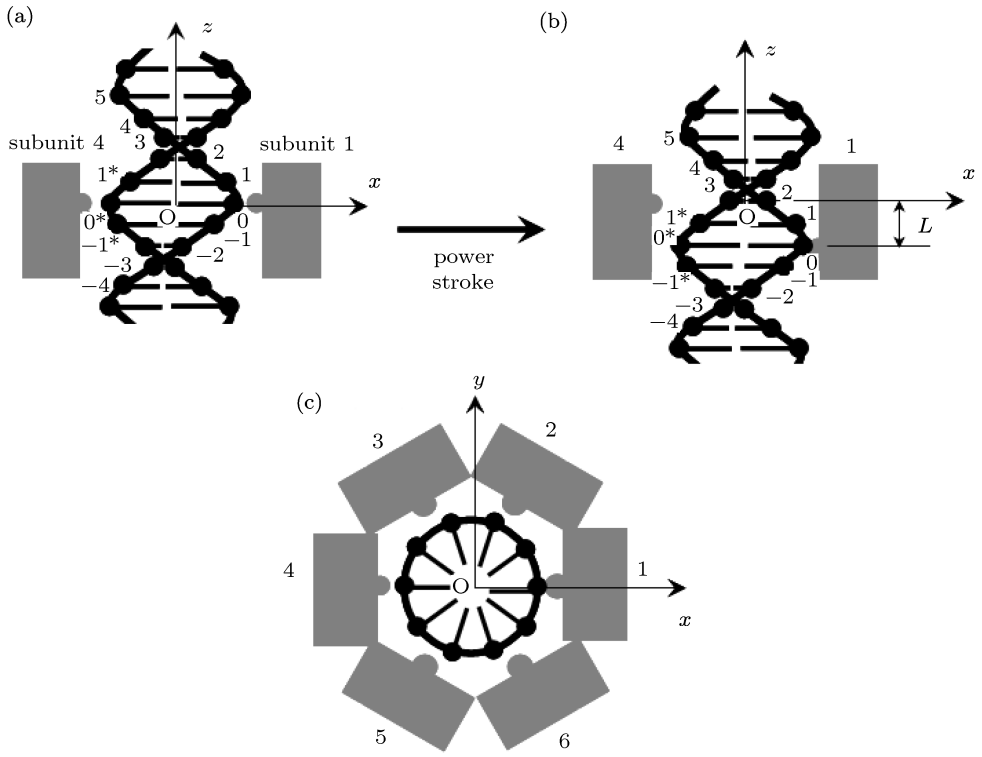


Fig.1. Schematic diagram for illustrating DNA translocation by six pRNA-ATPase subunits of the ϕ29 DNA packaging motor. (a) Side view of DNA, with Subunit1*.ATP complex binding strongly to one sugar and phosphate backbones of DNA, where for clarity only subunits 1 and 4 with their DNA-binding sites (grey dots) are drawn. (b) After hydrolysis of ATP in subunit 1, the rotation of its DNA-binding site drives DNA to move a distance L along the axis of the hexamer. (c) The plan view of (a).

Based on the three assumptions, our proposed mechanism of unidirectional DNA translocation by the ϕ29 DNA packaging motor is schematically shown in Fig.1. We begin with the Subunit1*.ATP complex binding strongly to one sugar and phosphate backbone of DNA (Fig.1(a)), which stimulates the transition of its next adjacent subunit 2 from Subunit2.ATP to the Subunit2*.ATP complex and simultaneously stimulates the ATP hydrolysis and Pi release in the Subunit1*.ATP complex (Assumption 2). The rotation of the DNA-binding site of subunit 1 induced by ATP hydrolysis drives DNA to move downwards by a distance L along the axis of the hexamer (Assumption 3) (Fig.1(b)). After Pi releases, subunit 1 becomes weakly bound to DNA. Now, due to the strong binding force of Subunit2*.ATP to DNA, subunit 2 binds

DNA. Note that the binding of Subunit2*.ATP to one sugar and phosphate backbone of DNA may induce its rotation around its helical axis. Thus, via hydrolysis of an ATP, the transfer of DNA from subunit 1 to subunit 2 results in DNA translocation by about L along the helical axis. To be consistent with available experimental data,[5,40] the power-stroke size is taken to be $L = 2$ bp. Here it is implicitly considered that the returned rotations of the DNA-binding site from a post-power-stroke position to a prepower-stroke position occur either following ADP release or following ATP binding. When Subunit2*.ATP is strongly binding DNA, the returned rotations of the DNA-binding site in other subunits have no effect on DNA translocation because in ADP and nucleotide-free states the subunits have weak binding affinities for DNA.

2.2. Kinetic pathway

In this mechanism (Fig.1), the main kinetic pathway in each subunit can be shown in Fig.2, where different states are connected by thick arrows. In the main pathway, $k_1 = k_{\rm b}^{(\rm ATP)}[\rm ATP]$ is the ATP-binding rate, k_2 (k_2') represents the transition rate from the unactivated Subunit.ATP complex to the activated Subunit*.ATP complex with (without) stimulation of its previous adjacent subunit bound strongly to DNA, k_3 (k_3') represents the ATP-hydrolysis rate of the subunit with (without) stimulation of its binding to DNA, and k_4 (k_4') represent the Pi-release rate from the subunit with (without) stimulation of its binding to DNA. Moreover, we denote k_5' as the ADP-release rate from the subunit when DNA is not bound to it, while k_5 as the ADP-release rate from the subunit when DNA is bound to it. In the presence of ADP, the binding of ADP to the nucleotide-free subunit is also included, with the binding rate denoted by $k_6 = k_{\rm b}^{(\rm ADP)}[\rm ADP]$. Note that, since the Subunit*.ATP and Subunit.ADP.Pi states are engaged strongly with DNA, it is supposed that the transition rates related to these two states, i.e., ATP-hydrolysis rate k_3 and Pi-release rate k_4, are dependent on an applied force acted on DNA, which follow the Arrhenius relation, $k_j = k_j^{(0)} \exp(-F\delta/k_{\rm B}T)$ ($j = 3, 4$), where $k_j^{(0)}$ is the rate under zero force, $\delta = 0.23$ nm is the characteristic distance and F represents either the internal force built up with capsid filling or the applied external force.

Besides the main kinetic pathway, as just mentioned above, two branched kinetic pathways can also occur in the mechanism, and are indicated by thin arrows in Fig.2. First, consider that two faced subunits (e.g., subunits 2 and 5 in Fig.1(c)) are transitioned to activated Subunit*.ATP states before the previous subunit 1 is transitioned to the weak Subunit.ADP state. Then it is possible that the two faced subunits can bind DNA simultaneously [Note1] after subunit 1 is transitioned to the weak Subunit.ADP state. If this occurs, the strong binding of one Subunit*.ATP complex to DNA resists the power stroke generated by another Subunit*.ATP complex. This is equivalent to a large force acting on the two subunits during the ATP-hydrolysis-induced power stroke. Thus, according to the Arrhenius relation, the ATP hydrolysis rate k_3 of the two subunits will be significantly reduced. For clarity, we denote the reduced ATP hydrolysis rate by k_7. As will be simulated below, the significant reduction of the ATP hydrolysis rate results in the occurrence of pauses. Second, consider that, after one subunit (e.g., subunit 1) that is bound to DNA is transitioned to the weak DNA-binding state, no other subunit is in the strong DNA-binding state. This may occur under the condition that the other subunit either (i) has not been transitioned to the activated Subunit*.ATP state or (ii) has completed ATP hydrolysis and has then become ADP or nucleotide-free state when subunit 1 is transitioned to the weak DNA-binding state. If this occurs, an external force on DNA can disengage DNA from the subunit 1 (see Subsection 2.3), which results in the occurrence of slips.

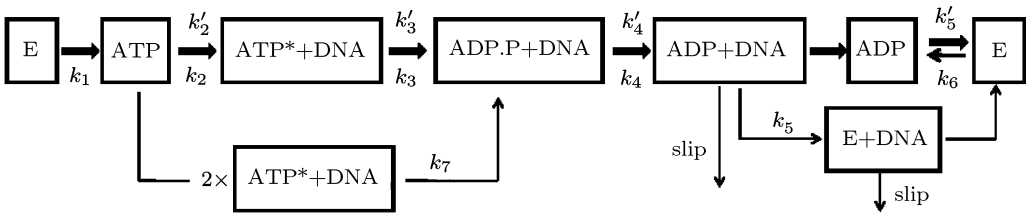


Fig.2. The kinetic pathway in each catalytic subunit.

2.3. Monte Carlo simulations

Based on the kinetic pathways (Fig.2), we let the model system evolve according to the Monte Carlo algorithm. The Monte Carlo method is a powerful one to simulate the kinetic cycle of a molecular motor,[41,42] because state transitions of motors are always stochastic. In our simulations, during each time step Δt ($\Delta t = 10^{-5}$ s in simulations), a random number x is generated with uniform probability between 0 and 1. If $x \leq P_i$, the transition k_i occurs; if $x > P_i$, the transition k_i does not occur, where $P_i = k_i \Delta t$ is the probability of state transition.

In our model, the interactions between pRNA-ATPase subunits and DNA in our simulations are described as follows. When only one subunit is in the strong DNA-binding state, the subunit binds the DNA. When two or more subunits are in the strong DNA-binding state and no two of them are faced with each other, the DNA is engaged with the subunit which is adjacent to the subunit that has just bound the DNA. When two or more subunits are in the strong DNA-binding state and there exist two of them in Subunit*.ATP states that are faced with each other, the two faced subunits bind the DNA simultaneously with a probability of $k_{\rm p} = 0.01$, while only one of the two subunits is engaged with DNA with a probability of $1 - k_{\rm p}$. Another consideration is that, after a subunit engaged with DNA becomes ADP or nucleotide-free state, if no other subunit becomes strong DNA-binding state (either Subunit*.ATP or Subunit.ADP.Pi state), the DNA can be disengaged from the subunit to which it is weakly bound and then slides relative to the hexamer under the action of the external force, because no subunit has a strong interaction with the DNA. In other words, a slip can occur. Since the subunit in ADP and nucleotide-free states has different binding affinities for DNA, we consider the detachment of DNA from the subunit separately. (i) When the subunit (e.g., subunit 1) engaged with DNA becomes ADP state, because of the weak binding affinity, DNA is still bound to subunit 1 for a while but can be disengaged from the subunit by an external force. According to Kramers,[43] the detaching rate of DNA from the subunit 1 to which it is weakly bound follows the relation $k_{\rm s} = k_{\rm s}^{(0)} \exp(F d_{\rm s}/k_{\rm B}T)$, with $k_{\rm s}^{(0)} = 0.1$ s^{-1} and $d_{\rm s} = 0.25$ nm. (ii) When subunit 1 becomes nucleotide free, because of a negligibly small binding affinity, DNA is supposed to be disengaged from the subunit once it becomes nucleotide free. In other words, when subunit 1 becomes nucleotide free the slip occurs definitely.

For the simulation, we take values of transition rate as shown in Table 1. From values of k_2', k_2, k_3', k_4', $k_3^{(0)}$ and $k_4^{(0)}$, it is noted that, during the main mechanochemical coupling cycle, the ATPase rate is enhanced about 24-fold in the presence of DNA, which is consistent with the available experimental data of about 20-fold.[44] Moreover, from values of $k_3^{(0)}$ and k_7, with relation $k_j = k_j^{(0)} \exp(-F\delta/k_{\rm B}T)$ ($k_j^{(0)} = k_3^{(0)}$ and $\delta = 0.23$ nm) it is estimated that the power-stroke force on DNA generated by a subunit is about 100 pN, which is larger than the measured stall force of about 60 pN.

Table 1. Kinetic parameters used in the simulation. (1 M=1 mol/L)

kinetic parameters	values	kinetic parameters	values
$k_{\rm b}^{(\rm ATP)}$/M^{-1}·s^{-1}	2×10^6	$k_3^{(0)}(=k_4^{(0)})$/s^{-1}	100
$k_{\rm b}^{(\rm ADP)}$/M^{-1}·s^{-1}	4×10^6	k_7/s^{-1}	0.25
k_2'/s^{-1}	10	k_5'/s^{-1}	50
k_2/s^{-1}	200	k_5/s^{-1}	0.02
$k_3'(=k_4')$/s^{-1}	4		

3. Results

Typical simulated traces of DNA translocation at a constant load of 5 pN under different values of [ATP] (5, 25, 100, 500 μM) and a fixed value of [ADP] (5 μM) are shows in Fig.3(a). It is clearly seen that the DNA translocation (or packaging) rate increases with the increase of [ATP]. It is also seen that slips and pauses occur occasionally during the DNA packaging, as observed experimentally. Next, we present our statistical results,

each datum of which is calculated from our simulation with a duration of 40 minutes.

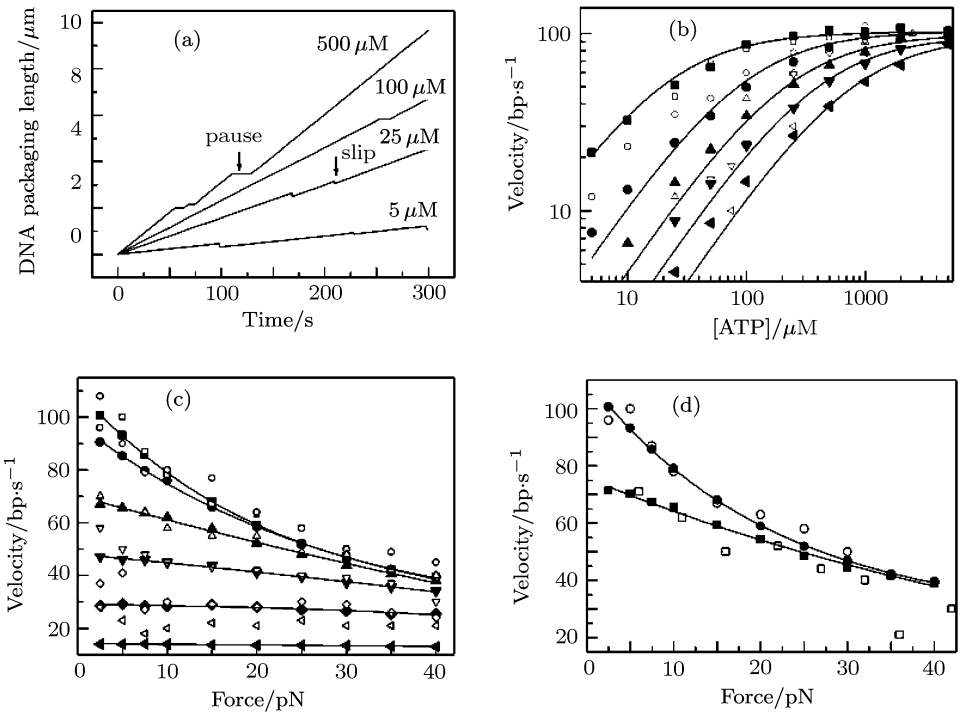


Fig.3. Dependences of packaging rate on [ATP] and [ADP] and on force. (a) Typical simulated traces of DNA translocation at a constant force of 5 pN and [ADP]=5 μM with different ATP concentrations: [ATP]=500, 100, 25, 5 μM. (b) Simulated results (filled symbols) of packaging rate versus [ATP] at a constant force of 5 pN with different ADP concentrations: [ADP]=5, 100, 250, 500, 1000 μM (square, circle, up-triangle, down-triangle, left-triangle, respectively). The unfilled symbols are the corresponding experimental data taken from Ref.[5]. (c) Simulated results (filled symbols) of packaging rate versus force at [ADP]=5 μM with different ATP concentrations: [ATP]=500, 250, 100, 50, 25, 10 μM (square, circle, up-triangle, down-triangle, diamond, left-triangle, respectively). The unfilled symbols are the corresponding experimental data taken from Ref.[5]. (d) Simulated results (filled symbols) of packaging rate versus force at [ATP]=500 μM with [ADP]=500 μM (square) and 5 μM (circle). The unfilled symbols are the corresponding experimental data taken from Ref.[5].

3.1. Packaging rate

In Fig.3(b), we show our simulated results for the packaging rate, v, versus [ATP] at different values of [ADP]. The results are in good agreement with the experimental data.[5] As Fig.3(b) shows, the dependence of the packaging rate on [ATP] at a fixed [ADP] follows the Michaelis–Menten equation $v = V_{\max}[\mathrm{ATP}]/(K_{\mathrm{M}} + [\mathrm{ATP}])$ (solid lines in Fig.3(b)).

To investigate the force dependence of the packaging rate, we simulate the force–velocity behaviour at different values of [ATP] (Fig.3(c)) and at different values of [ADP] (Fig.3(d)). Good agreement is obtained between the theoretical and experimental results.[5] As shown in Fig.3(c), at near-saturating [ATP] the packaging rate depends strongly on force. In this regime, the rate-limiting steps are the transitions with rates k_3 and k_4, which are dependent on force. However, at low values of [ATP], where the rate-limiting step is ATP binding (with transition rate k_1), the velocity becomes independent of force.

3.2. Pause

Previous experimental results[4] showed that pauses occur occasionally during packaging at a near-saturating [ATP], and its occurrence frequency increases with the increase of capsid filling. To compare our simulation with experiment on pauses, in our simulation we consider that, when DNA becomes stalled for more than 1 s, a pause event occurs. The simulated results of pause frequency versus percentage of DNA packaged are shown

in Fig.4(a), where the relation between external force and the percentage of DNA packaged is deduced from Fig.3(d) in Ref.[4]. It is seen that the simulation is in agreement with the experiment. It is noted that, in our simulation, the pause results from the significant reduction of the ATP-hydrolysis rate, which is induced by simultaneous binding of DNA by two faced subunits in Subunit*.ATP states.

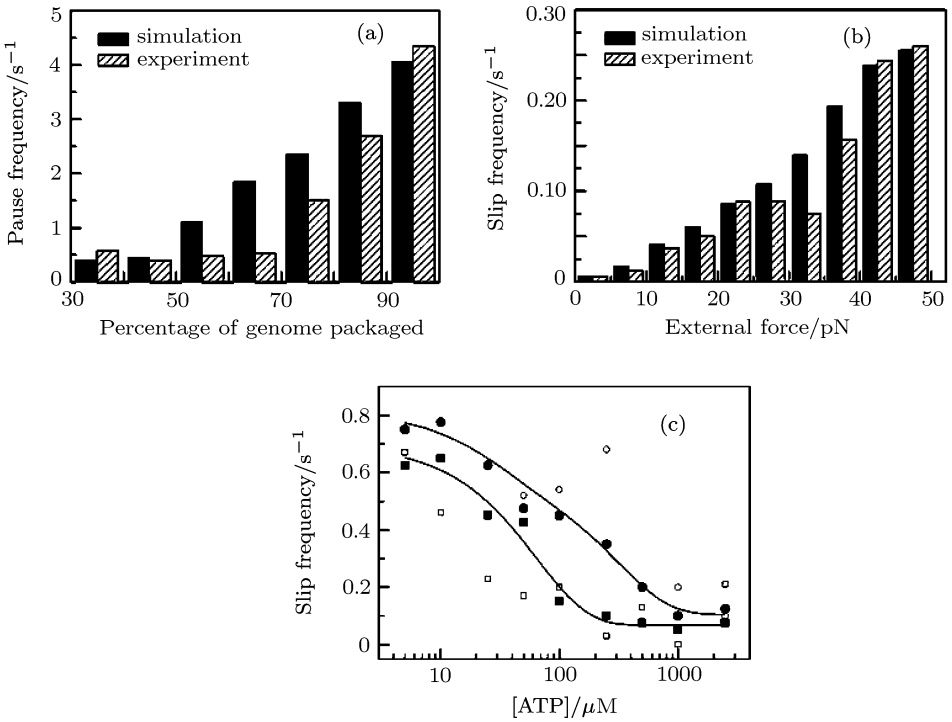


Fig.4. Pauses and slips. (a) Simulated and experimental results of pause frequency versus the amount of DNA packaged at [ATP]=500 μM and [ADP]=5 μM. The experimental data are taken from Ref.[4]. (b) Simulated and experimental results of slip distribution versus external force at [ATP]=500 μM and [ADP]= 5μM. The simulated results are obtained from 527 slipping events. The experimental data are taken from Ref.[4]. (c) Simulated results (filled symbols) of slip frequency versus ATP concentration at a constant force of 5 pN with [ADP]=5 μM (square) and 500 μM (circle). The unfilled symbols are the corresponding experimental data taken from Ref.[5].

3.3. Slip

As our model shows, when a subunit engaged with DNA becomes ADP or nucleotide-free state, if no other subunit becomes strong DNA-binding state (either Subunit*.ATP or Subunit.ADP.Pi state), the slip can occur when the DNA is acted by an external force. To test this argument, we simulated the slip frequency or distribution under various values of external force, [ATP] and [ADP]. The results for slip distribution versus the external force are shown in Fig.4(b). The results for slip frequency versus [ATP] under different values of [ADP] are shown in Fig.4(c). It is seen that the simulated results are indeed in good agreement with the experimental ones.[4,5]

3.4. Effect of nonhydrolyzable ATP analogue

In the above, we have simulated the packaging dynamics of the motor in the absence of nonhydrolyzable analogues. Now we study the effect of nonhydrolyzable analogues (e.g., AMP-PNP) on the packaging dynamics. For the simulation, we take the AMP-PNP-binding rate as $k_{\rm b}^{(\rm AMP-PNP)} = 1\times10^5 {\rm M}^{-1}\cdot{\rm s}^{-1}$ and the dissociation rate of AMP-PNP from Subunit*.AMP-PNP as 0.06 s^{-1}. Then using the same values of other transition rates as before, we simulate the pausing dynamics under different values of [ATP], [AMP-PNP] and F. The simulation results are summarized in Fig.5. It is seen that all the results are in good agreement with the experimental data.[5]

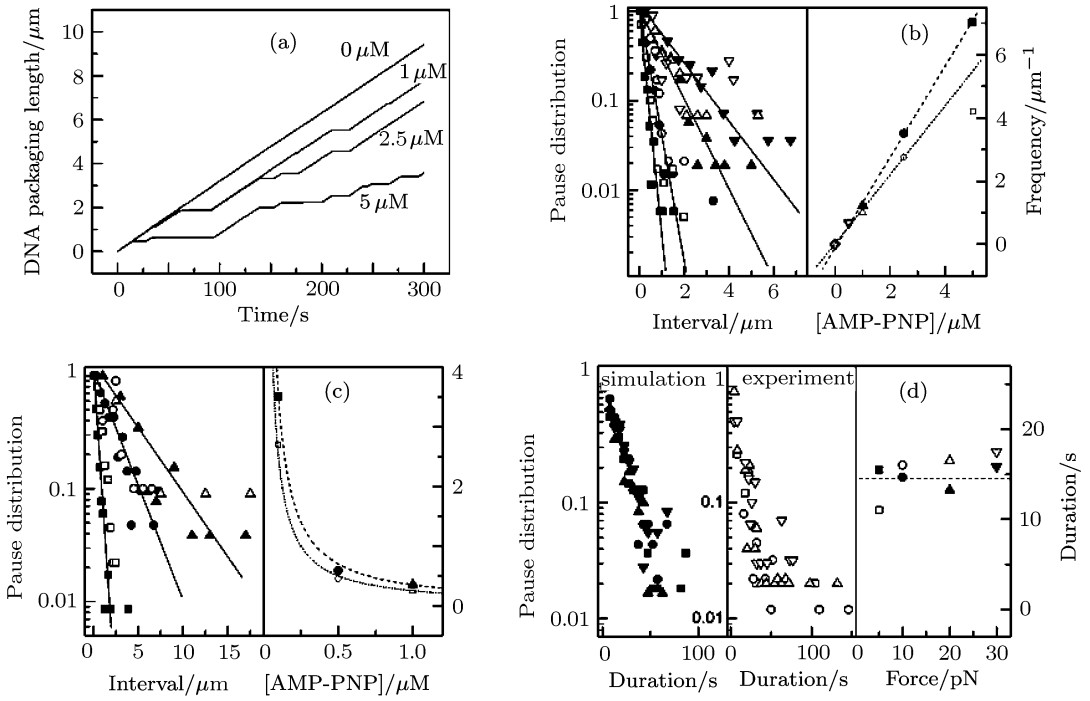


Fig.5. Pauses induced by AMP-PNP. (a) Typical simulated traces of DNA translocation at F=5 pN, [ATP]=100 μM and [ADP]=5 μM with different AMP-PNP concentrations: [AMP-PNP]=0, 1, 2.5, 5 μM. (b) Left panel: simulated (filled symbols) and experimental (unfilled symbols) results of normalized distribution of the pause interval at F=5 pN, [ATP]=100 μM and [ADP]=5 μM with different AMP-PNP concentrations: [AMP-PNP]=0.5, 1, 2.5, 5 μM (square, circle, up-triangle, down-triangle, respectively), with number of pauses counted in simulations of 5000 s duration: n = 83, 132, 252, 327, respectively. Right panel: mean pause frequency (pauses per μm packaged) versus [AMP-PNP] obtained from fitting to simulated (filled symbols) and experimental results (unfilled symbols). (c) Left panel: simulated (filled symbols) and experimental (unfilled symbols) results of normalized distribution of the pause interval at F = 5 pN, [AMP-PNP]=2.5 μM and [ADP]=5 μM with different ATP concentrations: [ATP]=100, 500, 1000 μM (square, circle, up-triangle, respectively), with number of pauses counted in simulations of 5000 s duration: n = 252, 93, 62, respectively. Right panel: mean pause frequency versus [ATP] obtained from fitting to simulated (filled symbols) and experimental results (unfilled symbols). (d) Simulated (left panel) and experimental (middle panel) results of normalized distribution of the pause duration at [AMP-PNP]=2.5 μM, [ATP]=100 μM and [ADP]=5 μM with different forces: F = 5, 10, 20, 30 pN (square, circle, up-triangle, down-triangle, respectively), with number of pauses counted in simulations of 5000 s duration: n = 180, 171, 189, 129, respectively. Right panel: mean pause duration versus force obtained from fitting to simulated (filled symbols) and experimental results (unfilled symbols). All experimental data are taken from Ref.[5].

3.5. Predicted results

It is important to predict the function that has not been characterized previously in order to further verify our model. Here, we use our simulations to predict the following:

(i) Figure 6(a) shows the pause frequency versus percentage of DNA packaged at various values of [ATP]. First, it is seen that, at low values of [ATP], the pause frequency increases with the increase of the percentage of DNA packaged, similar to that at saturating [ATP]. Second, it is seen that pause frequency decreases with the decrease of [ATP]. This can be understood as follows. As [ATP] decreases, the transition rate $k_1 = k_b^{(ATP)}$[ATP] decreases. Consequently, the probability decreases so that more than one subunits become strong DNA-binding states and also the two faced subunits become Subunit*.ATP states after the previous subunit becomes weak DNA-binding state, thus decreasing the pause frequency. The relation of the pause frequency versus percentage of DNA packaged at various values of [ADP] is shown in Fig.6(b). It is seen that the pause frequency decreases with the increase of [ADP]. This is because the increase of [ADP] reduces the probability that the two faced subunits become Subunit*.ATP states since

ADP is a competitive inhibitor to ATP.

(ii) Figure 6(c) shows the slip frequency versus external force at various values of [ATP]. As anticipated, at low values of [ATP], the slip frequency also increases with the increase of the external force, similar to that at saturating [ATP]. Moreover, it is noted that the slip frequency decreases with the increase of [ATP]. This is because the probability that no subunit becomes strong DNA-binding states decreases with the increase of [ATP]. Figure 6(d) shows the slip frequency versus external force at various values of [ADP]. It is seen that the ADP has the opposite effect to ATP (Fig.6(c)) on the slip frequency, because ADP is a competitive inhibitor to ATP.

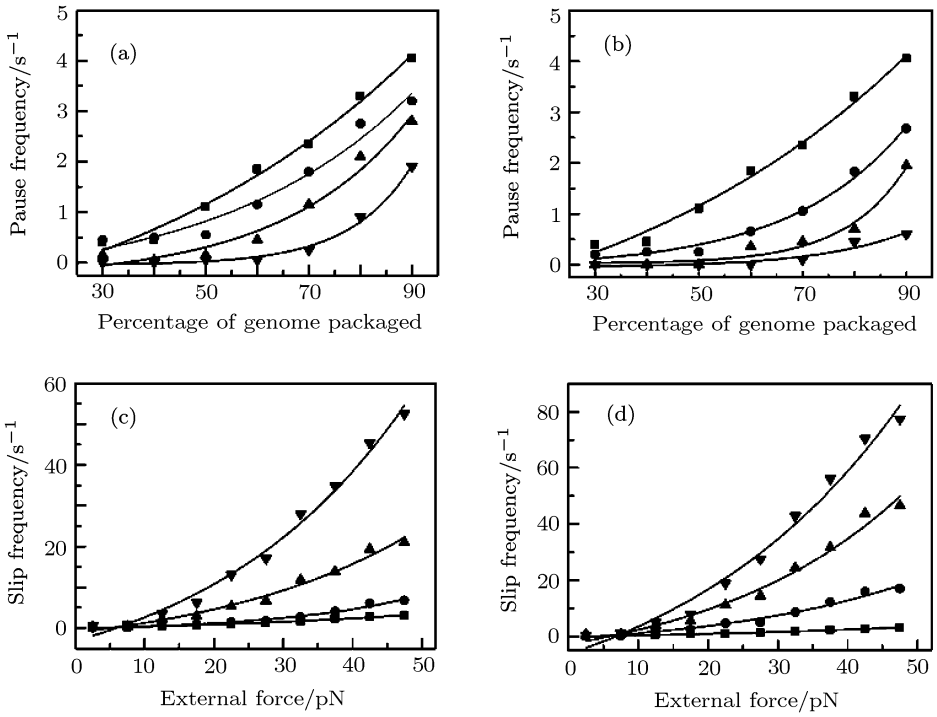


Fig.6. Predicted results for pauses and slips. (a) Pause frequency versus the amount of DNA packaged at [ADP]=5 μM and different ATP concentrations: [ATP]=500, 250, 100, 50 μM (square, circle, up-triangle, down-triangle, respectively). (b) Pause frequency versus the amount of DNA packaged at [ATP]=500 μM and different ADP concentrations: [ADP]=5, 100, 250, 500 μM (square, circle, up-triangle, down-triangle, respectively). (c) Slip frequency versus external force F at [ADP]=5 μM and different ATP concentrations: [ATP]=500, 250, 100, 50 μM (square, circle, up-triangle, down-triangle, respectively). (d) Slip frequency versus external force F at [ATP]=500 μM and different ADP concentrations: [ADP]=5, 100, 250, 500 μM (square, circle, up-triangle, down-triangle, respectively).

4. Discussion

4.1. Coordinated ATPase activities

In our model, one of the three assumptions is that the ATPase activities of the subunits are coordinated by the interaction with DNA (Assumption 2). To see the effect of this coordination on the dynamics of DNA translocation, in Fig.7 we show our simulated results of velocity versus k_2, k_3 and k_4, with other parameter values the same as those used before. It is seen that the packaging velocity decreases significantly with the decrease of k_3 and k_4. The packaging velocity also decreases with the decrease of k_2. Thus, the coordinated

ATPase activities around the ring are a prerequisite for high velocity of the packaging motor.

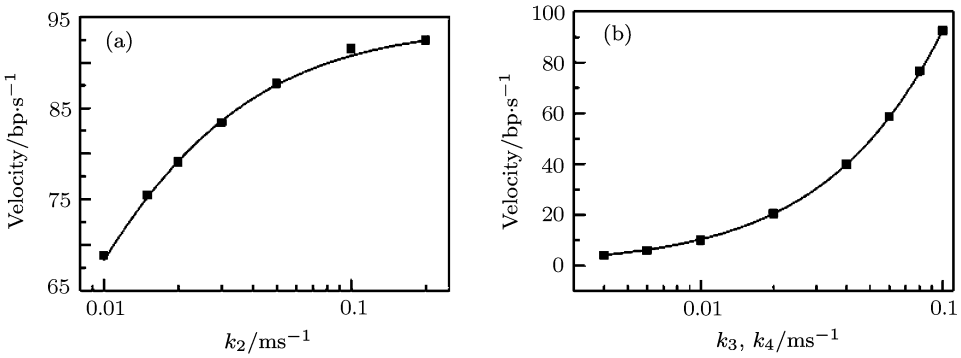


Fig.7. (a) Dependence of packaging rate on transition rate k_2 with [ATP]=500 μM and [ADP]=5 μM at a constant force of 5 pN. (b) Dependence of packaging rate on transition rates k_3 and k_4 with [ATP]=500 μM and [ADP]=5 μM.

Recently, Rickgauer *et al*[45,46] developed a ramped DNA stretching technique that can measure the velocity at near-zero loads. Their experiment reveals that the motor can generate significantly higher velocities ($v \approx 150$ bp/s) than detected previously. In our model, by increasing the values of parameters $k_3^{(0)}$ and $k_4^{(0)}$ and slightly increasing the value of δ while keeping the other parameters unchanged, we simulate their results very well (see Fig.8). The increases of $k_3^{(0)}$ and $k_4^{(0)}$ implies a higher coordination induced by the interaction with DNA.

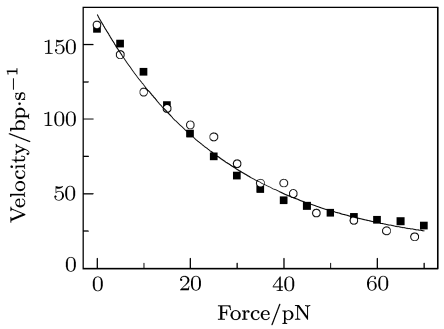


Fig.8. Packaging velocity versus force calculated with $k_3^{(0)} = k_4^{(0)} = 2200$ s^{-1} and $\delta = 0.25$ nm at [ATP]=500 μM and [ADP]=5 μM while other parameter values are same as those used in Fig.3. Filled symbols are simulated results while unfilled symbols are experimental data taken from Ref.[46].

4.2. Stepwise manner of DNA packaging

Very recently, by using high-resolution optical tweezers, Moffitt *et al*[47] observed that the packaging of DNA by the ϕ29 DNA packaging motor does not occur uniformly but occurs in a stepwise manner consisting of 'dwells', in which the DNA length remains constant, followed by 'bursts', in which DNA is translocated in ∼10-bp increments. To quantitatively explain this phenomenon, we modify our model by making a further assumption. Because the hexamer is assembled from three dimers,[12] it is possible that the three pairs may have different kinetic properties from each other. Here we assume that, of the six subunits, a pair of subunits (e.g., subunits 1 and 2) have different kinetic properties from other four subunits, i.e., subunits 1 and 2 have a different ATP binding rate from the other four subunits and cannot hydrolyze ATP. The kinetic parameters for subunits 1 and 2 and those for the other four subunits are shown in Table 2. The ATP-release rate for subunits 1 and 2 is $k_{\rm release}^{\rm (ATP)}$. In our simulations, the rate $k_{\rm release}^{\rm (ATP)}$ for subunits 1 and 2 is independent of F. The ATP-hydrolysis rate k_3 and Pi-release rate k_4 of other four subunits follow the Arrhenius relation, $k_j = k_j^{(0)} \exp(-F\delta/k_{\rm B}T)$ $(j = 3, 4)$, where $\delta = 0.7$ nm. When two or more subunits are in the strong DNA-binding state and there exist two of them in Subunit*.ATP states that are faced with each other, the two faced subunits bind the DNA simultaneously with a probability of $k_{\rm p} = 0.08$. The detaching rate of DNA from one Subunit.ADP complex or Subunit.ATP complex to which it is weakly bound also follows the relation $k_{\rm s} = k_{\rm s}^{(0)} \exp(Fd_{\rm s}/k_{\rm B}T)$, with $k_{\rm s}^{(0)} = 0.12$ s^{-1} and $d_{\rm s} = 0.11$ nm.

Table 2. Kinetic parameters used in the simulations.

parameters for subunits 1 and 2		parameters for other four subunits	
kinetic parameter	value	kinetic parameter	value
$k_b^{(ATP)}/M^{-1}\cdot s^{-1}$	0.2×10^6	$k_b^{(ATP)}/M^{-1}\cdot s^{-1}$	2×10^6
k_2'/s^{-1}	0.5	k_2'/s^{-1}	0.5
k_2/s^{-1}	30	k_2/s^{-1}	200
$k_{release}^{(ATP)}/s^{-1}$	60	$k_3'(k_4')/s^{-1}$	4
k_7/s^{-1}	0.25	$k_3^{(0)}(k_4^{(0)})/s^{-1}$	1700
k_5'/s^{-1}	50	k_7/s^{-1}	0.25
k_5/s^{-1}	0.01	k_5'/s^{-1}	50
$k_b^{(ADP)}/M^{-1}\cdot s^{-1}$	0.4×10^6	k_5/s^{-1}	0.01
		$k_b^{(ADP)}/M^{-1}\cdot s^{-1}$	4×10^6

Taking the kinetic parameters as given in Table 2, we show in Fig.9(a) some typical simulated traces of DNA translocation at a constant force of 8 pN with different values of [ATP].[Note2] The traces resemble the experimental ones well. From the calculations, we noted that, during each dwell period, multiple ATP molecules bind before the burst occurs, while during the burst period, the four ATP molecules bound to subunits 3, 4, 5 and 6 are sequentially hydrolyzed, thus giving four sequential power strokes. These are consistent with the analyses of Moffitt *et al*,[47] showing that multiple ATPs bind during each dwell. The statistical results of mean dwell time and burst time versus [ATP] are shown in Fig.9(b), and are also in good agreement with the experimental results.[47] Note that, using these values of parameters in Table 2, the previously observed results of DNA packaging rate versus [ATP] and force and of pause and slip frequencies versus [ATP] and force[4,5] can also be well simulated.

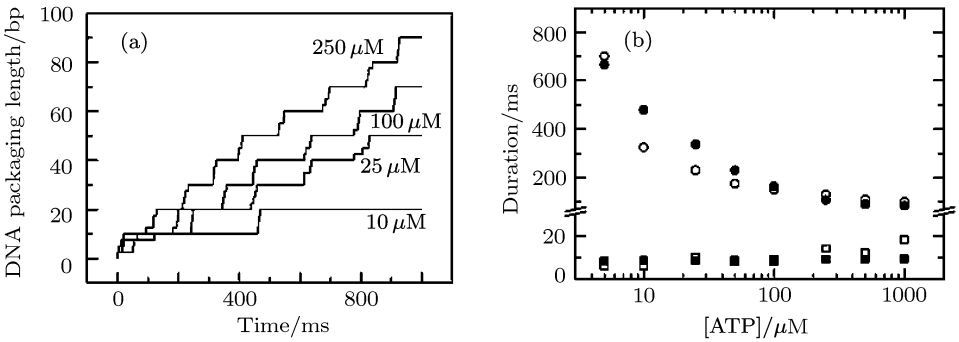


Fig.9. Simulated results for stepwise DNA packaging. (a) Typical simulated traces of DNA translocation at a constant force of 8 pN and [ADP]=5 μM with different ATP concentrations: [ATP]=250, 100, 25, 10 μM. (b) Simulated results (filled symbols) of mean dwell time (circle) and burst time (square) at a constant force of 8 pN and [ADP]=5 μM for all [ATP] concentrations. The unfilled symbols are the corresponding experimental data taken from Ref.[47].

4.3. Origin of pauses

The origin of inherent pauses occurring during packaging is still unclear. In the literature, at least two possible explanations for pauses have been proposed.[48] (i) Resistance by the DNA already packaged causes a stall in the motion of the DNA until the packaged region of the DNA molecule rearranges. However, the motor does not diminish its DNA-driving force during the stall. (ii) There is a 'particular state' during the kinetic cycle of the six subunits of packaging motor which can cause a stall. The first one is not a good explanation for the pause, because if the resistance by the DNA already packaged causes the pause, the pause duration should increase with the packaged DNA length, as shown by Ali *et al*.[22] However, Smith *et al*[4] found that the duration of pauses is almost uncorrelated with how much DNA is packaged even though the pausing frequency increases with the increase of capsid filling.

Although the second one is a possible best explanation for pauses, the origin for the occurrence of the 'particular state' has not been determined. Serwer[48] proposed that the 'particular state', or 'the zero-motion state', may result from the binding of DNA by the small accessory protein. Here, our simulation shows that the 'particular state' is the state when the two faced subunits in Subunit*.ATP states bind DNA simultaneously. When this occurs, the power stroke generated by one subunit is resisted by the strong binding to DNA by another subunit. According to the Arrhenius relation, this will greatly reduce the ATP-hydrolysis rates k_3 of the two subunits, and thus result in a long period of stalled state, i.e., a pause occurs.

The great reduction of transition rate k_3 is dependent on the power-stroke force on DNA that the subunit can generate, which is in turn determined by the binding force to DNA by a Subunit*.ATP complex. Since this binding force is unrelated to the resistance force by the DNA already packaged in the capsid, the duration of pauses is uncorrelated with how much DNA is packaged. However, as the capsid filling increases, the transition rate of k_3 and k_4 of the subunit (e.g., subunit n) engaged with DNA decreases. Consequently, the time of subunit n engaged with DNA in Subunit*.ATP and Subunit.ADP.Pi states increases while the rates of other subunits becoming Subunit*.ATP states are unchanged. Thus, the probability for the two faced subunits to become Subunit*.ATP states increases when subunit n has become ADP state. As a result, the pause frequency increases with the increase of capsid filling (see Fig.4(a)), which is consistent with experimental results.[4] Note that, in our model, we have not considered the interaction between the connector and DNA, because the inner radius of the ϕ29 connector channel (no less than 1.8 nm) is wider than the radius of ds-DNA ($\sim$ 1.0 nm) and the frictional resistance between them is negligible, as shown by Serwer.[48]

4.4. Origin of slips

A slip occurs when a subunit engaged with DNA is transitioned to the weak DNA-binding state while no other subunit is in the strong DNA-binding state. In the model, this can occur when the other subunit either (i) has not been transitioned to the activated Subunit*.ATP state or (ii) has completed ATP hydrolysis and then released products (Pi or ADP) and/or has been bound by ADP via a transition with rate k_6 (see pathway in Fig.2). As [ATP] increases, the probability for the occurrence of situation (i) is reduced, thus the slip frequency decreases (see Fig.4(c)). As [ADP] increases, the probability for the occurrence of situation (ii) is increased, thus the slip frequency increases (see Fig.4(c)). Since the detaching rate k_s (see Subsection 2.3) of DNA from the subunit.ADP complex increases with the increase of F, it is expected that the slip frequency would increase with the increase of F (see Fig.4(b)).

5. Conclusion

Based on our proposed model for DNA packaging by the ϕ29 DNA packaging motor, the Monte Carlo simulation results can reproduce nearly all the experimentally determined features available. In order to have a high packaging velocity and high mechanochemical coupling efficiency, coordination of ATPase activities between pRNA-ATPase subunits is required. Our simulation shows that a pause results from a significant reduction of the ATP hydrolysis rate when the two faced subunits in Subunit*.ATP states strongly bind DNA simultaneously. When a subunit engaged with DNA becomes ADP or nucleotide-free state, while no other subunit becomes strong DNA-binding state (either Subunit*.ATP or Subunit.ADP.Pi state), a slip can occur when the DNA is acted on by an external force. Moreover, we present some predictions of motor function, which are expected to be tested in future experiments. Finally, we believe that the theoretical method presented here can be easily applied to other ring-shaped molecular motors, such as T7 helicase, RuvB protein and the P4 packaging motor.

Acknowledgments

We thank Drs. J.R. Moffitt, K. Aathavan, Y.R. Chemla and C. Bustamante for providing experimental data and a paper (Moffitt *et al*[47]) before publication.

Footnotes

Note 1. It is noted that only the two faced subunits can bind DNA simultaneously due to the structure of double-stranded DNA. Two adjacent or alternate subunits cannot bind DNA at the same time, because, if this happened, too large atorsional torque would be produced!

Note 2. As the experiment shows,[47] we take the power-stroke size by ATP hydrolysis to be 2.5 bp here.

References

[1] Earnshaw W C and Casjens S R 1980 *Cell* **21** 319
[2] Black L W 1989 *Ann. Rev. Microbiol.* **43** 267
[3] Grimes S, Jardine P J and Anderson D 2002 *Adv. Virus. Res.* **58** 255
[4] Smith D E, Tans S J, Smith S B, Grimes S, Anderson D L and Bustamante C 2001 *Nature* **413** 748
[5] Chemla Y R, Aathavan K, Michaelis J, Grimes S, Jardine P J, Anderson D L and Bustamante C 2005 *Cell* **122** 683
[6] Simpson A A, Tao Y, Leiman P G, Badasso M O, He Y, Jardine P J, Olson N H, Morais M C, Grimes S, Anderson D L, Baker T S and Rossmann M G 2000 *Nature* **408** 745
[7] Guasch A, Pous J, Ibarra B, Gomis-Ruth F X, Valpuesta J M, Sousa N, Carrascosa J L and Coll M 2002 *J. Mol. Biol.* **315** 663
[8] Morais M C, Tao Y, Olson N H, Grimes S, Jardine P J, Anderson D L, Baker T S and Rossmann M G 2001 *J. Struct. Biol.* **135** 38
[9] Zhang F, Lemieux S, Wu X, St.-Arnaud D, McMurray C T, Major F and Anderson D L 1998 *Mol. Cell* **2** 141
[10] Chen C and Guo P 1997 *J. Virol.* **71** 3864
[11] Ibarra B, Caston J R, Llorca O, Valle M, Valpuesta J M and Carrascosa J L 2000 *J. Mol. Biol.* **298** 807
[12] Shu D, Zhang H, Jin J and Guo P 2007 *EMBO J.* **26** 527
[13] Guo P, Zhang C, Chen C, Trottier M and Garver K 1998 *Mol. Cell* **2** 149
[14] Lee T J and Guo P 2006 *J. Mol. Biol.* **356** 589
[15] Hendrix R W 1978 *Proc. Natl. Acad. Sci. USA* **75** 4779
[16] Riemer S C and Bloomfield V A 1978 *Biopolymers* **17** 785
[17] Kindt J, Tzlil S, Ben-Shaul A and Gelbart W M 2001 *Proc. Natl. Acad. Sci. USA* **98** 13671
[18] Purohit P K, Kondev J and Phillips R 2003 *Proc. Natl. Acad. Sci. USA* **100** 3173
[19] Tzlil S, Kindt J T, Gelbart W M and Ben-Shaul A 2003 *Biophys. J.* **84** 1616
[20] Marenduzzo D and Micheletti C 2003 *J. Mol. Biol.* **330** 485
[21] LaMarque J C, Le T and Harvey S C 2004 *Biopolymers* **73** 348
[22] Ali I, Marenduzzo D and Yeomans J M 2004 *J. Chem. Phys.* **121** 8635
[23] Purohit P K, Inamdar M N, Grayson P D, Squires T M, Kondev J and Phillips R 2005 *Biophys. J.* **88** 851
[24] Spakowitz A J and Wang Z G 2005 *Biophys. J.* **88** 3912
[25] Ali I, Marenduzzo D and Yeomans J M 2006 *Phys. Rev. Lett.* **96** 208102
[26] Petrov A S and Harvey S C 2007 *Structure* **15** 21
[27] Hugel T, Michaelis J, Hetherington C L, Jardine P J, Grimes S, Walter J M, Falk W, Anderson D L and Bustamante C 2007 *PLoS Biol.* **5** e59
[28] Muller B, Tsaneva I R and West S C 1993 *J. Biol. Chem.* **268** 17185
[29] Hingorani M M and Patel S S 1993 *Biochemistry* **32** 12478
[30] Singleton M, Sawaya M, Ellenberger T and Wigley D 2000 *Cell* **101** 589
[31] Liao J C, Jeong Y J, Kim D E, Patel S S and Oster G 2005 *J. Mol. Biol.* **350** 452
[32] Crampton D J, Mukherjee S and Richardson C C 2006 *Mol. Cell* **21** 165
[33] Mancini E J, Kainov D E, Grimes J M, Tuma R, Bamford D H and Stuart D L 2004 *Cell* **118** 743
[34] Kainov D E, Tuma R and Mancini E J 2006 *Cell. Mol. Life Sci.* **63** 1095
[35] Ibarra B, Valpuesta J M and Carrascosa J L 2001 *Nucleic Acids Res.* **29** 4264
[36] Xie P 2007 *Biochim. Biophys. Acta* **1774** 737.
[37] Xie P 2007 *J. Theor. Biol.* **249** 566
[38] Crampton D J, Guo S, Johnson D E and Richardson C C 2004 *Proc. Natl. Acad. Sci. USA* **101** 4373
[39] Hishida T, Han Y W, Fujimoto S, Iwasaki H and Shinagawa H 2004 *Proc. Natl. Acad. Sci. USA* **101** 9573
[40] Guo P X, Peterson C and Anderson D L 1987 *J. Mol. Biol.* **197** 229
[41] Singh M P, Mallik R, Gross S P and Yu C C 2005 *Proc. Natl. Acad. Sci. USA* **102** 12059
[42] Chen Y D, Yan B and Rubin R J 2002 *Biophys. J.* **83** 2360
[43] Kramers H A 1940 *Physika* **7** 284
[44] Ibarra B, Valpuesta J M and Carrascosa J L 2001 *Nucleic Acids Res.* **29** 4264
[45] Fuller D N, Rickgauer J P, Jardine P J, Grimes S, Anderson D L and Smith D E 2007 *Proc. Natl. Acad. Sci. USA* **104** 11245
[46] Rickgauer J P, Fuller D N, Grimes S, Jardine P J, Anderson D L and Smith D E 2008 *Biophys. J.* **94** 159
[47] Moffitt J R, Chemla Y R, Aathavan K, Grimes S, Jardine P J, Anderson D L and Bustamanre C 2009 *Nature* **457** 446
[48] Serwer P 2003 *J. Struct. Biol.* **141** 179